Geophysical characterization of karst landscapes in Kentucky as modern analogs for paleokarst reservoirs

Michael T. May[1] and Thomas B. Brackman[2]

Abstract

Subsurface interpretation of paleokarst reservoirs is greatly aided by 3D seismic and other modern modeling tools and the inherent complexity of productive reservoirs requires an understanding of reservoir heterogeneities and compartmentalization. Such complexity also requires a review of karst processes and development, which can be beneficially captured via geophysical characterization of near-surface karst landscape features that certainly equate to our better understanding of high-side oil productive areas. Both electrical resistivity tomography (ERT) and refraction microtremor (ReMi) geophysical surveys at the Green River Preserve adjacent to Mammoth Cave National Park in the Mississippian Ste. Genevieve and Girkin Limestones are providing details of karst features, including horizontal passages, uvulas or karst valleys, sinkholes (dolines), vertical pits or dome caves, and associated karst system infill. Geophysical anomalies include reversals of shear-wave velocities in a domal (pit) cave, and an inferred bedding-plane controlled conduit system associated with a drained sinkhole basin. Other anomalies detected in the shallow subsurface include large contrasts in geoelectrical measurements near the sinkhole basin interpreted also as a cave or conduit system. In contrast to anomalies, a mappable continuity of ERT and ReMi transects along the Green River suggests bedrock joints controlling the linear nature of bedrock highs and lows, similar to a series of grikes and clints that typify the south-central Kentucky karst.

Introduction

Karst regions provide special locations in which to view and study depositional and diagenetic facies in carbonates as well as to link solution enlarged joints, fractures, and mappable cave passage orientation to crustal stress conditions and ultimately to regional tectonic regimes. In the Mammoth Cave National Park region of south-central Kentucky, there are hundreds of kilometers of subterranean exposures, providing advantages for study of the 3D aspects of carbonate facies. Furthermore, study of such karst systems in the context of weathering, sequence-boundary development, and associated facies provide valuable modern analogs (e.g., Loucks, 2001) for better understanding of ancient karstic petroleum reservoirs. There are many ancient karst reservoir examples such as the Ordovician Ellenburger (e.g., see Kerans, 1988) and Permian San Andres (Tinker et al., 1995; Craig, 1988; Nissen et al., 2008) of west Texas, and the Cambro-Ordovician Knox of Kentucky and Tennessee (Anderson, 1991).

East of the Mammoth Cave system with a mapped length of 645 km (approximately 400 miles) is the Green River Preserve (GRP) typified by outcrops of Mississippian carbonates (Figures 1–3). This is a property managed by Western Kentucky University consisting of almost 1508 acres (610 hectares) situated proximal to Mammoth Cave National Park (53,000 acres or 21,448 hectares). This karstland region is perhaps one of the world's most extensively studied and possesses the largest network of mapped cave passages on our planet (e.g., Brucker and Watson, 1976; Palmer, 1981, 1991; Borden and Brucker, 2000). Near the GRP in Mammoth Cave National Park, several hydrogeologic studies have been conducted (e.g., Quinlan and Ray, 1981, 1989; Ray and Currens, 1998; Meiman et al., 2001) and there have also been investigations of cave-fill sediment (e.g., Granger et al., 2001; White, 2007) and the mineralogical nature of the terra rossa soils typified by karst regions (e.g., Merino and Banerjee, 2008). The Mammoth Cave region (Figure 3), however, has been little studied in regard to geophysical anomalies associated with karst features and allied weathering and sedimentological events representing approximately two million years of earth's history. Four to five levels of cave passages developed during this two-million-year period are reflective of eustatic sea-level rise and fall and con-

[1]Western Kentucky University, Geography and Geology, Bowling Green, Kentucky, USA. E-mail: michael.may@wku.edu.
[2]Northern Kentucky University, Center for Integrative Natural Science and Mathematics, Highland Heights, Kentucky, USA. E-mail: brackmant1@nku.edu.

Manuscript received by the Editor 19 November 2013; revised manuscript received 30 April 2014; published online 31 July 2014. This paper appears in *Interpretation*, Vol. 2, No. 3 (August 2014); p. SF51–SF63, 8 FIGS., 1 TABLE.
http://dx.doi.org/10.1190/INT-2013-0179.1.

comitant base-level changes of the Green River, development of regolith zones, soil formation, and deposition and erosion of sediment (Palmer, 1987; Jacoby et al., 2011). Studies have been conducted of paleocave carbonate reservoirs, their origins, their complexities, and changes related to their respective depositional basin histories (e.g., Loucks, 1999). Our study contributes and emphasizes mappable trends associated with early development of karstic reservoirs.

This study at the GRP is one of the first in the region that has combined ERT and ReMi geophysical surveys to provide details of karst features including horizontal passages, uvulas or karst valleys, sinkholes (dolines), vertical pits or dome caves, and associated fluids and sediment associated with infilling of karst features. Such a study provides the basis for better understanding paleokarst reservoirs that are of great importance in hydrocarbon provinces throughout the world. This study provides ERT and ReMi data and relates them to the most obvious structural features such as tectonically controlled joints, fractures, grikes, and clints but also to other complexities associated with karst reservoirs (e.g., see Kerans, 1988). Less-obvious features may include karst breakdown or brecciated zones, or limestone "floater blocks" (e.g., Merino and Banerjee, 2008). Clints are blocky protrusions of limestone and in contrast, grikes represent fissures or fractures between clints in karst terrains. Grikes (kluftkarren) have been well documented for years (e.g., Sweeting, 1973) and they may be enlarged and can extend in subparallel linear patterns for many meters until they terminate or are covered by surface sediment or soils. Breakdown zones are important features associated with collapse or the brecciated karst systems that are typically a combination of rock and terra rossa soils.

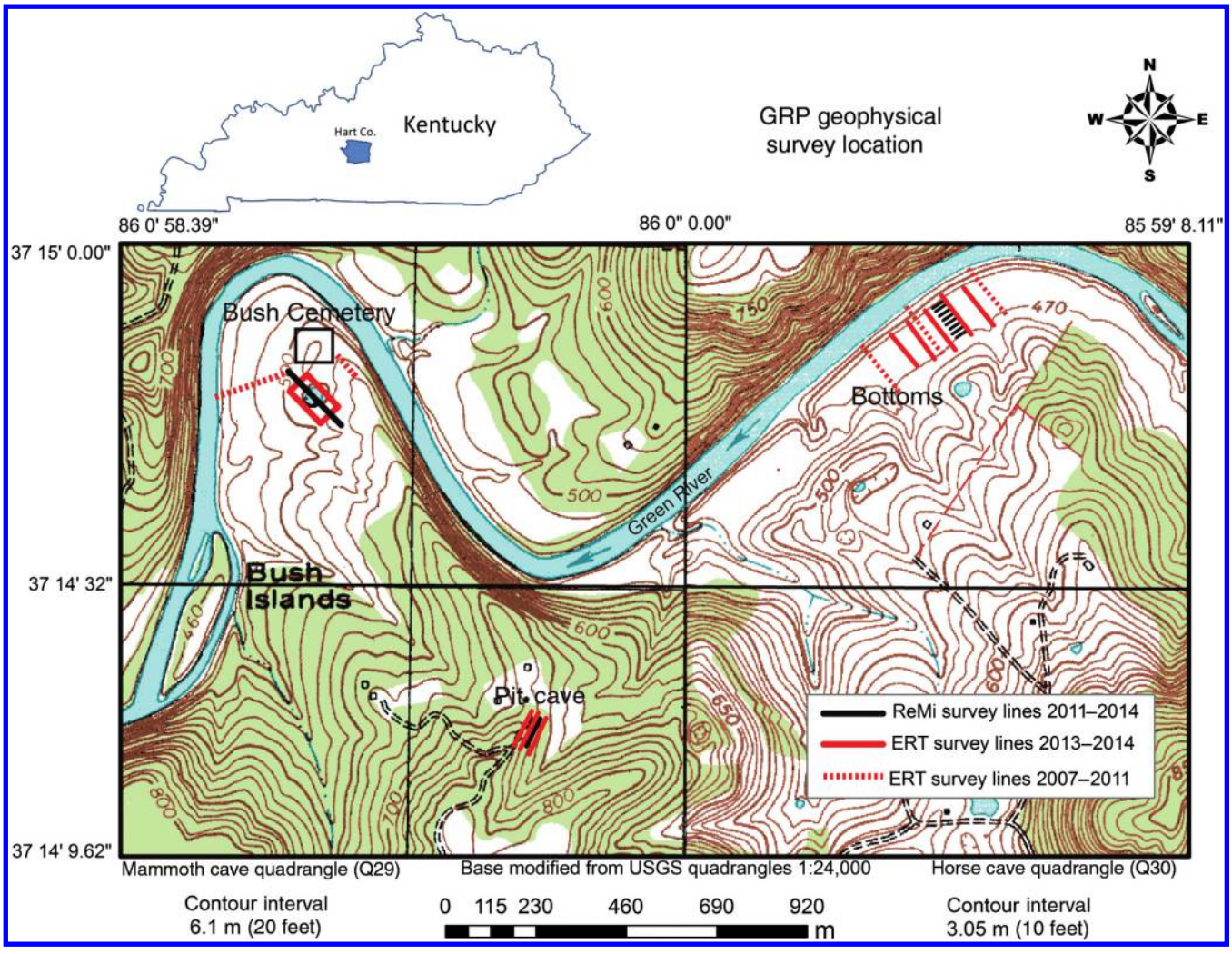

Figure 1. GRP near-surface geophysics study sites. Red lines show 2D electric resistivity tomography (ERT) surveys from 2013 to 2014. Dashed red lines show 2D ERT surveys from 2007 during an extended drought and also from 2011. Red rectangle south of Bush Cemetery in former (drained) pond area indicates location of 3D ERT survey of 2013. Black lines indicate location of refraction microtremor (ReMi) lines from 2011 in the former pond area, 2013 in the pit cave area, and in 2014 in the river bottoms area. Mammoth Cave National Park is located just to left of this view. Inset map shows location of Hart County and Kentucky, in which the GRP is situated.

Study sites at Green River Preserve

Location and stratigraphy

The Illinois Basin (or Eastern Interior Basin) extends over much of Illinois, western and southwestern Indiana, and western to south central Kentucky and can be characterized as an intracratonic basin with broad arches but with concentrated regions of folds and faults (e.g., Nelson, 1990). Many of these concentrations of folds and faults are associated with hydrocarbon prospective locations and conventional weight oil. The southeastern periphery of the basin in the Mammoth Cave region contains conventional and unconventional hydrocarbons in relatively shallow to outcropping Mississippian (Chesterian) and basal Pennsylvanian sandstone (e.g., Noger, 1987; May and Kuehn, 2009; May, 2013). The stratigraphy of the southeast portion of the basin includes rather thick Middle Mississippian carbonates, overlain by more cyclic and mixed siliciclastic and carbonate Chesterian series units. Chesterian units are primarily overlain unconformably by Pennsylvanian siliciclastic rocks (Figure 3). Mammoth Cave, a world heritage site, is developed within the Middle Mississippian limestone units, including the St. Louis Limestone and the Ste. Genevieve Limestone (Figure 2), and comprises the classic karst plain which dominates the region. Other stratigraphic units that exhibit karst features in the area include the Girkin Limestone (Golconda Group) (Figure 2) and the Haney Limestone (Figure 3).

Study sites at the GRP include use of ERT and ReMi at several test location sites. Sites include areas traversing the alluvial bottoms of the Green River (Qal), over a pit cave in an upland area, and over a former (drained via karst collapse) pond bordering but superjacent to the Green River alluvial bottomland (Figures 1 and 3). All of these sites rest on Middle Mississippian Limestone (see Figure 2 for specific stratigraphic position). Most of the test beds were located atop soil and sediment (i.e., terra rossa) above the Ste. Genevieve Limestone with the higher elevation areas surveyed within Girkin Limestone and underlying Ste. Genevieve Limestone (Figure 3).

Methods of data acquisition

Electric resistivity tomography

Electric resistivity is one of the most widely varying of the physical properties of natural materials. Certain minerals, such as native metals and graphite, conduct electricity via the passage of electrons; however, electronic conduction is generally very rare in the subsurface. Most minerals and rocks are insulators, and electric current preferentially travels through the double layer and water-filled pores in soils and rocks by the passage of the free ions in pore waters (i.e., ionic conduction). It thus follows that the degree of saturation, interconnected porosity, and water chemistry (i.e., total dissolved solids) are the major controlling variables of the resistivity of soils and rocks. In general, electric resistivity directly varies with changes in these parameters. Fine-grained sediments, particularly clay-rich sediments such as glacial till, are excellent conductors of electricity, whereas sands and gravels are much

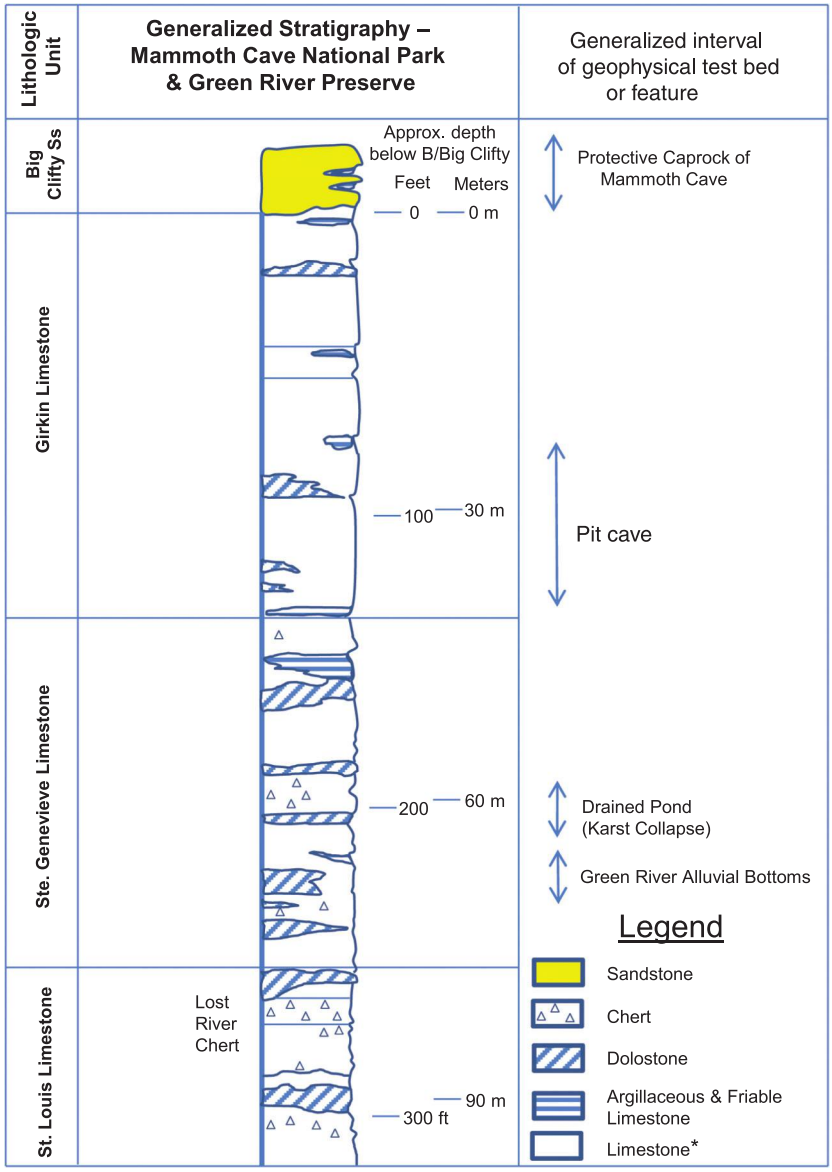

Figure 2. Mississippian stratigraphy in the Mammoth Cave region (based on Figure 7 in Toomey and Olson [2008]: USGS Field Guide). For more regional stratigraphic context including Chesterian rocks and basal Pennsylvanian see May (2013) and Figure 3. *Designates undifferentiated limestone ranging from wackestone to grainstone.

more resistive. Carbonate rocks (i.e., limestone and dolomite) are very electrically resistive when they are unfractured, but can have significantly lower resistivity values when fractured and/or weathered and solutioned.

The galvanic-source method, a subset of electric geophysical methods, traditionally uses a low-frequency alternating current applied through a pair of electrodes and the potential difference is measured at a pair of receiver electrodes (Zonge cited in Butler, 2005). Ohm's law controls the relationship between the electric resistivity, current, and the electric potential (Loke et al., 2013). In a continuous medium, Ohm's law and conservation of current (Poisson's equation), are normally used to calculate the potential (Loke et al., 2013). In the forward problem, the potential due to a point current source located at x_s is given by

$$\nabla \cdot \left[\frac{1}{\rho(x,y,z)}\nabla\varphi(x,y,z)\right] = -\frac{\partial j_c}{\partial t}\delta(x_s), \qquad (1)$$

where ρ is the resistivity, φ is the potential, and j_c is the charge density (Loke et al., 2013). For the simplest inverse problem, the current I and voltage ΔV measurements are converted into an apparent resistivity ρ_a value using

$$\rho_a = k\frac{\Delta V}{I}, \qquad (2)$$

where k is the geometric factor that depends on the configuration of the current and potential electrodes (Koefoed, 1979).

ERT involves the collection of numerous, four-point resistivity measurements, using strings of multiple electrode cables to create a high-resolution image of the planar image created by the array configuration (Zonge cited in Butler, 2005).

There have been significant improvements in the past quarter century for direct-current geoelectric imaging methods that are commercially available as noted by Loke et al. (2013). There are also many applications to near-surface imaging including considerations of hydraulic conductivity in the context of petrophysics and aquifer geometry (Slater, 2007) and low-frequency methods for subsurface characterization and aquifer monitoring (Revil et al., 2012).

The expectation for using ERT in karst terrains is that collected and analyzed field data would necessarily suggest that over short distances, either laterally or vertically, that porosity and permeability are quite varied as there is geologic heterogeneity. Such heterogeneity is typically associated with a series of solution-enlarged fracture or conjugate joint sets (i.e., clints and grikes) near the surface (see, e.g., Quinlan and Ewers, 1981; Kerans, 1988) plus solution cavity or cave breakdown resulting in variable resistivity. This is common for the Mississippian bedrock at the GRP or within the south-central Kentucky karst.

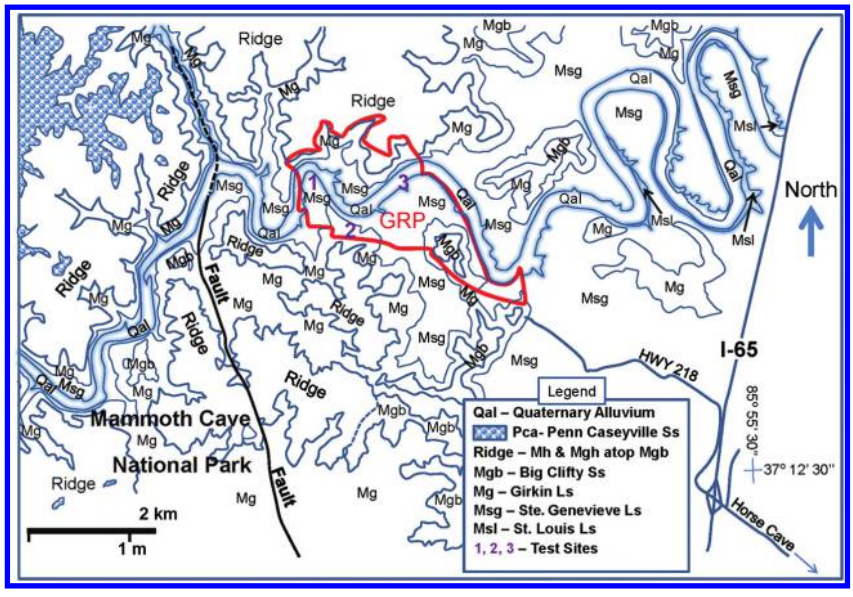

Figure 3. Location map of main (1200 acre) portion of GRP shown in context of surface bedrock geology and Qal (within glow lines) along Green River and adjacent Mammoth Cave National Park (park boundary approximates fault trace south of Green River and just east of fault north of river). Stratigraphic units include in ascending stratigraphic order. St. Louis Limestone (note arrows pointing to east part of view along Green River and I-65), Ste. Genevieve Limestone (Msg), Girkin Limestone (Mg), Big Clifty Sandstone (Mgb), Haney Limestone (Mh), Hardinsburg Sandstone (Mgh), and the unconformably overlying basal Pennsylvanian Caseyville Sandstone/Conglomerate (Pca) capping highest elevations in western part of view. Designation of "ridge" is for combination of Mgb, Mh, and Mgh for clarity (bolder lines); other ridge formers are designated by Mgb in the case in which it is the sole stratigraphic unit above karstified units (basal Mgb also bold lines). Dashed bold line separates ridge from Mgb ridge in the south central part of map. Test areas: (1) drained pond, (2) pit cave, and (3) Green River bottoms. Base modified from Kentucky Geological Survey interactive map service accessed November 2013.

Refraction microtremor

ReMi is a surface-wave seismic method for measuring in situ S-wave velocity profiles (Louie, 2001). The ReMi method was originally used to determine S-wave velocity profiles for International Building Code seismic site classification (Louie, 2001). The Rayleigh wave method has been used for delineation of landslides (Brackman et al., 2011a) and tunnel assessment (Brackman et al., 2011b), soil-compaction control, mapping the subsurface and estimating the strength of subsurface materials (Rucker, 2007).

The ReMi method uses the dispersive nature of Rayleigh waves to determine

the conditions of the subsurface. A 2D, slowness-frequency (p-f) transform of a microtremor record separates Rayleigh waves from other arrivals, allowing recognition of true-phase velocity against apparent velocities (Louie, 2001). Rayleigh waves are a combination of P- and SV-waves and only occur on a free surface. The depth of wave penetration is velocity/frequency dependent with generally higher frequencies penetrating the shallow portion of the subsurface and lower frequencies penetrating much deeper. In a homogenous, isotropic system the varying frequencies travel with the same velocity and are not dispersive. In applied field surveys, it is considered normal that the velocity of the subsurface tends to increase with depth and thus, Rayleigh waves will disperse by frequency. If a low-/high-velocity zone is present at depth, the "normal" dispersion curve is shifted by the zone. Thus, low-velocity zones, blind to refraction, are imaged. Individual wavelengths may encounter differing velocities because they pass through the measured section of the subsurface. If the impedance of a section is greater than a quarter of the wavelength, the wave is modified (Joyner et al., 1981; Boore, 2003). The resulting dispersion curve, however, is an average of the frequency velocity over the length of the array which must be taken into account during the interpretation phase.

Testing is performed at the surface using a standard refraction exploration seismometer and 4.5–10 Hz vertical P-wave geophones with up to 8-m spacing — thus, the use of the term "refraction" in refraction microtremor. The seismic source consists of ambient seismic "noise," or microtremors, which are constantly being generated by cultural and natural sources. The data acquisition procedure consists of obtaining 10–20, 30-second seismic noise records. During data collection, noise can be generated by walking the geophone line, jumping up and down at one end of the line, or dropping heavy objects. If possible, energy should be propagated along the length of the line and not from the side (Louie, 2001). Sources such as a 10-lb sledgehammer and steel plate tend to impart too much energy into the system for these investigations unless used at a distance greater than 10 times the geophone spacing. Much of the energy-source parameters are site dependent, and the use of multiple sources during data collection is advisable. Depending on the material properties of the subsurface, ReMi can determine S-wave velocities down to a minimum of 40 m (130 ft) and a maximum of 100 m (300 ft) depth (Louie, 2001) with array aperture limiting resolution at depth (Liu et al., 2000).

The wavefield transformation of the noise record involves a three-step procedure:

1) The first step is the p-τ transformation described by Thorson and Claerbout (1985). The transformation uses multiple records from seismograms, and converts them to amplitudes relative to the ray parameter p and an intercept time tau (Louie, 2001):

$$A(p = p0 + ldp, \tau = kdt) = \Sigma A(x = jdx, t = idt = \tau + px). \quad (3)$$

2) The second step uses the Fourier transformation of McMechan and Yedlin (1981) and takes each p-tau trace in $A(p,\tau)$ and computes its complex Fourier transform $F_A(p,f)$ in the tau or intercept time direction:

$$F_A(p,f = mdf) = \Sigma A(p,\tau = kdt)e^{i2\pi mdfkdt}. \quad (4)$$

3) The third step entails velocity spectral analysis of Louie (2001). The power spectrum $S_A(p,f)$, the magnitude squared of the complex Fourier transform, sums together in forward and reverse directions two p-tau transforms of a record:

$$S_A(p,f) = F_A^*(p,f)F_A(p,f). \quad (5)$$

Energy from the forward and reverse directions represents the absolute value of p, |p|, and is summed into one slowness axis completing the transform of a record:

$$S_A(|p|,f) = [S_A(p,f)]_{p>=0} + [S_A(-p,f)]_{p<0}, \quad (6)$$

individual records of p-f images $S_{An}(|p|,f)$ are added into an image of summed power:

$$S_{\text{total}}(|p|,f) = \sum_n S_{An}(|p|,f), \quad (7)$$

the analysis produces a record of the total spectral power S_{total} from a site and reveals the S-wave dispersion curve. The S-wave dispersion curve from the wavefield transformation is then manually selected and forward modeled to determine the subsurface S-wave velocity profile (Louie, 2001). The site-class definitions published by the International Code Council (2000) (see Table 1) are correlated with S-wave velocities and provide a broad description of the subsurface materials present. The

Table 1. National Earthquake Hazard Reduction Program substrate types based on S-wave velocity.

Site class	Soil profile name	Average properties in top 30 m (100 ft) (as per 2000 IBC section 1615.1.5) soil S-wave velocity V_S	
		ft/s	m/s
A	Hard rock	$V_S > 5000$	$V_S > 1524$
B	Rock	$2500 < V_S \leq 5000$	$762 < V_S \leq 1524$
C	Very dense soil and soft rock	$1200 < V_S \leq 2500$	$366 < V_S \leq 762$
D	Stiff soil profile	$600 < V_S \leq 1200$	$183 < V_S \leq 366$
E	Soft soil profile	$V_S < 600$	$V_S < 183$

site-class definitions are used to delineate subsurface materials in this paper.

Geophysical test beds

Drained pond

This significantly large doline or sink basin developed in the Ste. Genevieve Limestone (note stratigraphic position in Figure 2) near Bush Islands and Bush Cemetery on the GRP (Figures 1 and 3) at one time held water as is noted on the U.S.G.S. topographic map (Figure 1). The sink basin is presently dry after the base of the pond drained and discharged into a subterranean system, most probably into a bedding plane controlled conduit in the Ste. Genevieve Limestone. Geophysical surveys conducted across and in the vicinity of this feature included ReMi and ERT. The 2013 survey was set up to incorporate a 3D ERT array centered over the ReMi work conducted in 2011 (Figures 1 and 4). Additional work in the vicinity of the doline with 2D ERT lines in 2009 (area west of collapsed doline with karst infill material) and in 2013 (area northeast of doline as seen in map view of upper part of Figure 4) provide additional characterization of the subsurface near the drained pond. The 2009 transect that runs from the Green River toward the northeast shows the typical rise in elevation of the karstified bedrock surface but at the extreme northeast end of the traverse at depth there is a relatively lower resistivity detected. This anomaly is interpreted as the peripheral portion of the inferred conduit located also with the 3D ERT survey and ReMi survey. Similarly, there is yet another anomaly at depth near the center of the 2D ERT transect located most proximal to Bush Cemetery or to the northeast of the collapsed doline. Study of this ERT line also suggests that there is an opening or void below (Figure 4).

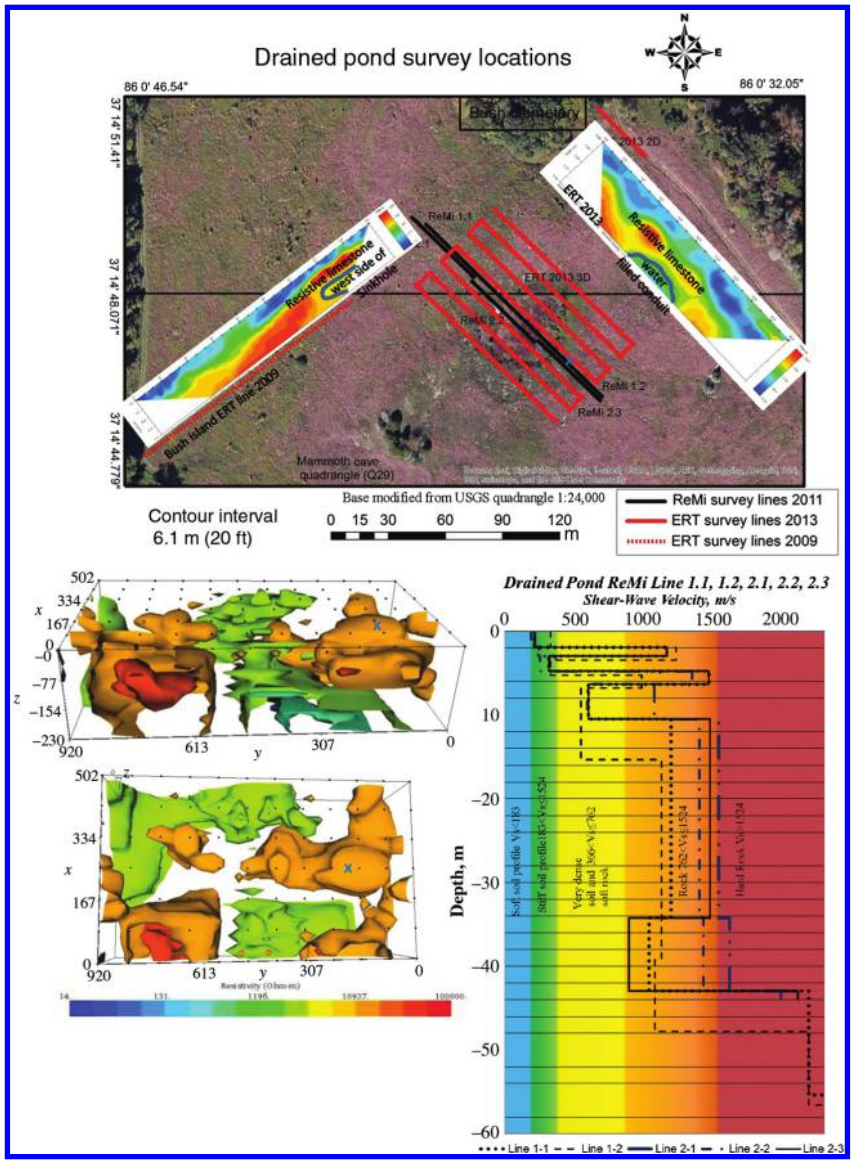

Figure 4. Drained pond GRP sinkhole. Map in upper view — red lines show 2D and 3D ERT surveys and black lines show ReMi seismic lines. Two ERT profiles plotted on map in upper view also. Three-dimensional survey: 84 electrodes, 9 m (30 ft) spacing, 4 m (15 ft) resolution. The X is for location reference of 3D surveys and green indicates lower resistivity correlating with karst infill material (lower left). Corresponding ReMi S-wave velocity profile shown in lower right.

In March 2011, five ReMi lines were conducted over the centerline of the drained pond and data were collected using a DAQ link 2, 24 bit data, 12-channel seismic acquisition unit with VScope software. SeisOpt® ReMi™ software was used to process, pick dispersion curves, and forward model the curves into a S-wave velocity profile. Lines 1.1 and 1.2 were conducted with 12 10-Hz geophones with 8-m (26.2 ft) spacing. Line 1.1 was conducted from the northwest side of the drained pond toward the center of the pond. Geophone 5 of line 1.1 was used as the origin of line 1.2, geophone 1 and was in line with line 1.1 and started near the center of the drained pond. Lines 1.1 and 1.2 indicate two large S-wave velocity reversals above 35 m and an additional one below 35 m (lower right part of Figure 4). The first reversal occurs between 3 and 5 m below the surface with an upper layer of approximately 1200 m/s (rock), 300 m/s (stiff soil) for the reversal, and returns to almost 1500 m/s (hard rock boundary). Approximately 2 m below the hard rock surface is another reversal of 4 m possessing a 600 m/s velocity (very dense soil and soft rock) increasing to 1200 m/s (rock) just below 10 m from the surface. A 150 m/s 10-m reversal can be seen below 35 m.

At nearly 43 m, the bedrock has a 2200 m/s (hard rock) S-wave velocity. Line 1.2 indicates the uppermost reversals are still present but the velocity values are lower. The 4-m reversal has increased to almost 8 m and the deep reversal is much smaller (50 m/s) and is close to experimental error.

In an effort to provide data redundancy and higher resolution of the subsurface of the drained pond, an additional three ReMi lines were conducted using the exact same equipment except with 4-m spacing. Geophone 1 from line 2.3 was positioned at geophone 12 from line 1.2 and retraced line 1.2. Geophone 1 from line 2.2 corresponded to geophone 12 line 2.3 and was positioned between geophone six and seven of line 1.2 and geophone 1 from line 2.1 corresponded to geophone 12 of line 2.2 and geophone 1 of line 1.2 and geophone 5 of line 1.1.

Lines 1.1, 1.2, and 2.3 display similar trends. Examination of the records indicate much of the upper and lower reversals are controlled by features at the end of line 1.1, the midsection of line 1.2, and the end of line 2.3, possibly placing the karst conduit believed to be responsible for draining the pond at a location just southeast of the center of the pond.

A 3D ERT survey was conducted in 2013 using Advanced Geosciences Inc.'s SuperSting R8/IP earth resistivity meter and EarthImager 3D software for data processing and inversion with 9.1 m (30 ft) spacing using 84 electrodes. The survey provided a macro view of the drained pond's subsurface. With 9.1-m spacing, resolution of subsurface features was limited to approximately 4.5 m near the surface and increasing with depth. Gross features of the pond indicate an infilling of karst voids in the vicinity of the ReMi anomaly.

Pit cave

The pit cave location (e.g., Figures 1 and 5) is one of the many documented karst features at the GRP. The cave at this location has been explored with its extent somewhat known but no formal mapping has been conducted as of this writing. This pit cave is believed to have developed along a vertical fracture or joint that was solution enlarged within the Girkin Limestone (for stratigraphic position see Figure 2). The extent of connecting lateral passages or a passage that intersects this pit or dome cave feature is not known. The base of this pit (estimated to be approximately 21 m [70 ft]) is several meters above the contact with the underlying Ste. Genevieve Limestone. There are several caves in the region that have hundreds of meters long lateral passages near the Ste. Genevieve-Girkin contact such as the Forestville Saltpeter Cave on the north bank of the Green River (D. Applegate, personal communication, 2013).

In April 2013, one ReMi line with 12, 10-Hz geophones with a 1.52 m (5 ft) spacing was conducted over the northwest side of the pit cave. Data were collected using a DAQLink II, 24-bit data, 12-channel seismic acquisition unit with VScope software. SeisOpt ReMi software was used to process, pick dispersion curves and forward model the curves into a S-wave velocity profile. The ERT data were collected in March 2014 using Advanced Geosciences Inc. SuperSting R8/IP earth resistivity meter and 24 electrodes with 1.53-m spacing. Three lines were conducted: Line 1 was conducted on the southeast side of the pit cave, line 2 was conducted 4.57 m (15 ft) on the opposite side of the pit and in line with the previous ReMi survey, and line 3 was conducted an additional 4.57 m (15 ft) to the northwest of ERT line two and the previous ReMi line. The S-wave velocity record was truncated near 15 m (50 ft) as a result of the 1.5 m (5 ft) geophone spacing and, therefore, not able to image the deeper sections of the pit cave (Figure 5). ERT and ReMi data were limited in length due to space constraints. The pit cave is located in heavily wooded areas and borders an uncooperative landowner.

One ERT cross section (line 1) over the pit cave shown in Figure 5 clearly delineates the shaft at 60 m (electrode 14) and the ReMi data (left side of Figure 5)

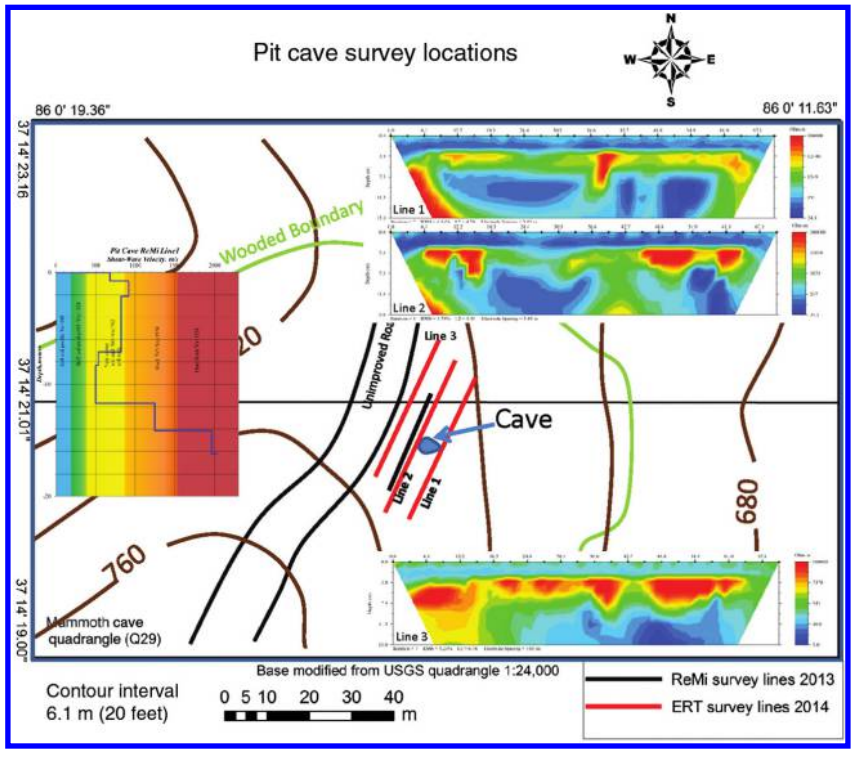

Figure 5. Topographic map of area surrounding pit cave with ERT and ReMi survey lines. ERT profiles 1–3 are shown in right and ReMi model in left. View on left side shows S-wave velocity with reversal indicating the upper part of the pit. For location of pit cave relative to GRP, see Figures 1 and 3.

corroborate the existence of a void with an obvious S-wave reversal 7–12 m below the surface. Line 2 also indicates a shaft at 60 m (electrode 14) and visual inspection of the pit from the surface shows a large passage striking in the direction of the resistive feature at depth. Line 3 indicates the passage continues toward the west as noted by a highly resistive area at 7.5 m deep and at 61 m on the surface traverse.

Dome or pit caves in the Mammoth Cave region are typically 10 m across (30 ft) and can be as much as 60 m (200 ft) from their top to bottom (Palmer, 1987). Geophysical data collected at the site indicate pit caves described by (Palmer, 1987) are present on the site.

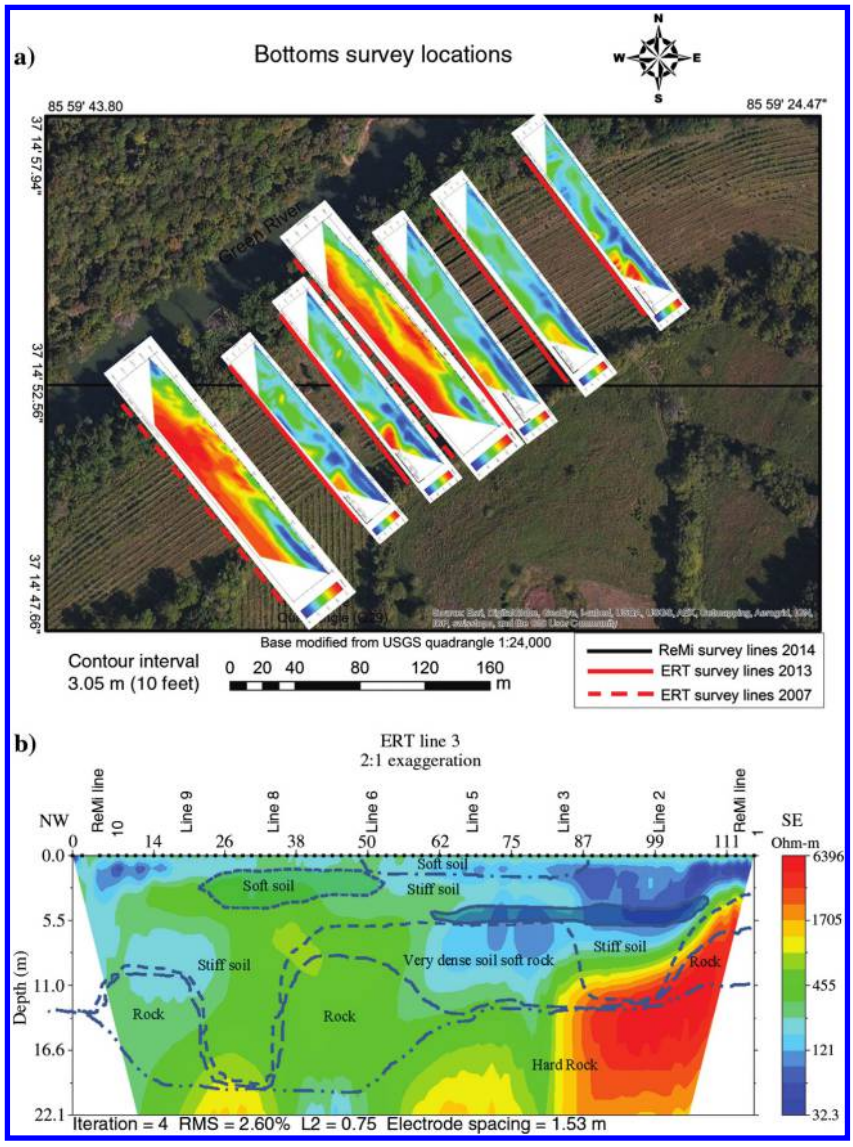

Figure 6. (a) GRP upstream Green River alluvial bottoms. Red lines show 2D ERT surveys from 2013 during wet period. Dashed red lines show 2D ERT surveys from 2007 during an extended drought. For the 2013 2D survey: 3 ft spacing, 1.5 ft resolution; blue indicates lower resistivity correlating with karst-infill material. Notice resistive material is more prevalent in the 2007 lines due to dry conditions; however, sediment infilled area is still visible. Cluster of ReMi lines (solid black lines) conducted in early 2014 between ERT lines 3 and 4. ReMi line 1 is to the SE and line 10 is to the northwest. ReMi lines 4 and 7 omitted for clarity. See Figure 6b for discussion and (b) lithologic interpretation based on The National Earthquake Hazard Reduction Program classification (see Table 1) of S-wave velocity data from ReMi survey cluster overlain on ERT line 3 profile in Green River alluvial bottoms (see Figure 1 for orientation). ReMi data were modeled using a priori depth values derived from ERT resistivity contrasts. The northwest extent is adjacent to the Green River. A low-velocity reversal between 62 and 110 m at a depth of 5.5 m is interpreted to be a porous medium supplying water to the surrounding area.

Green River alluvial bottoms

Two separate years are represented by ERT data collection in the Green River bottoms, November 2007 and October 2013 (see Figures 1 and 3 for location of bottoms and Figure 2 for stratigraphic position of bottoms in the Ste. Genevieve Limestone). The 2007 data were collected using Advanced Geosciences, Inc., Sting R1 earth-resistivity meter and 28 electrodes with 4.57-m spacing. Data were processed and a 2D inversion was performed using AGI EarthImager software. The 2013 data were collected using Advanced Geosciences Inc. SuperSting R8/IP earth-resistivity meter and 64–74 electrodes with 1.53-m spacing. As Figure 6a shows, a series of three lines were obtained in the drought year of 2007 (only two shown for clarity), and a series of five lines were acquired in the high-precipitation year of 2013. These data were collected essentially perpendicular to the straight reach of the Green River, traversing from proximal river locations, and in some cases down the riverbank and across the alluvial bottoms toward the southeast (mapped as Qal in Figure 3). As noted by several workers, it is possible to monitor changes in aquifers (e.g., Revil et al., 2012) and interpret several properties of the subsurface such as soil moisture and clay content via translation of geoelectric measurements (Schwartz et al., 2008; Loke et al., 2013).

A series of 10 ReMi lines were conducted in the early spring of 2014 perpendicular and between ERT lines 3 and 4 to capture a series of S-wave velocity profiles. The profiles assist in determining depth to bedrock and identify low-velocity zones (voids) that may be present. The ReMi data were collected using a DAQLink III, 24-bit data, 24-channel seismic acquisition unit with VScope software. SeisOpt ReMi software was used to process, select dispersion curves and forward model

the curves into a S-wave velocity profile. Twenty-four, 10-Hz geophones at 1.2 m (4 ft) spacing were used. A 1.2-m spacing was chosen to provide better resolution of data in the near surface because the ERT lines indicated features of interest at less than 22 m depth (Figure 6b).

The ReMi data were modeled using a priori depth values from the ERT survey data and were determined by choosing depths derived from contrast between resistivity values. Areas where warm colors transitioned into cool colors were considered a boundary between resistive rock and possible overburden. Areas, where the cool colors were intense were considered as an upper and lower transition zone. These transition zones were applied to the ReMi models and the velocities were forward modeled. The models were extremely easy to fit to the data as a result. The resulting S-wave velocity profiles were superimposed on the ERT lines and velocity isopach lines constructed (see Figure 6b). The contours indicate hard rock (see Table 1) at depth transitioning to slower materials. In the region of cool colors on the southeast end of the ERT line, a velocity reversal is clearly delineated. This is interpreted as a water-filled porous lens possibly composed of a gravel or coarse sand. The reversal/conductive region is assumed to supply water to this area and keeps the area saturated even in severe drought periods (see discussion below). The addition of the ReMi data and the a priori information from the ERT data assisted in improving the interpretation of the subsurface.

The ERT transects exhibit a similar pattern throughout the sequence (Figure 6a). The display of similarity, except for resistivity values, is remarkable because the lines had been collected six years apart in a drought versus wet weather conditions. For example, the 2007 data reflect dry conditions and a highly resistive substrate as noted by warm colors, whereas the 2013 data reflect a much more subdued series of values but still not exhibiting cool coloration (Figure 6a and 6b). Inspection of these transects reveals that all measured lines across the alluvial bottoms reflect a relatively more conductive shallow substrate nearest the Green River. Moving southeasterly, the ERT traces show a relatively shallow, resistive substrate, followed by a wide zone of conductive material near the southeastern terminus overlying a distinctly higher resistive layer. This highly resistive layer, at least under relatively wet conditions, even shows "digitate" signatures suggestive of solution-enlarged channels into the Ste. Genevieve Limestone. Such "invasion" of cooler colors suggests a tomographic view not unlike what would be expected in evolution of epikarst features with development of separated, highly resistive, solid rock bodies (e.g., see Figure 7a and 7b). It is also interesting to note that a more smooth (or less digitate) inferred bedrock surface shown by the 2007 transects is exhibited because the spacing on the electrodes was 4.6 m (15 ft) versus 0.46 m (3 ft) spacing on transects run in 2013. Furthermore, the lack of water in the shallow subsurface could have also made the resistivity contrast less between solid bedrock and solution-enlarged channels or grikes.

Modern analogs for ancient reservoirs

Discussion in the above section of geophysical test beds referred to in Figures 4 and 6 (e.g., sinkhole and alluvial bottoms) clearly shows the study of modern karst systems in a geophysical sense with data collection nodes being spaced even 4.6 m (15 ft) apart reveals a very punctuated aquifer, or reservoir in the making. Additionally, closer spaced nodes for data collection provide higher resolution models for geologic heterogeneity typified by karst. Nissen et al. (2008) stress the need for using a whole suite of production, core, downhole geophysical log, and 3D seismic data in characterizing ancient karst reservoirs to elucidate the characteristics and spatial distribution of inherently complex karst oil fields (e.g., San Andres of West Texas). Similarly, our geophysical characterization of modern karst and associated near-surface features has relied on multiple 2D and 3D arrays to best image bedrock relief, sediment infills (breakdown, floater blocks, terra rossa soils, brecciated zones, chute cutoff sediments from the Green River etc.) which can potentially be not only highly porous but also highly permeable.

Understanding the modern development of karst and its continuity (as in linear features recorded in this study along the Green River), as well as abrupt variation vertically and laterally (as in the case of pit caves and horizontal passages also noted in this study), provides insight into the role such systems play for porosity and permeability enhancement or destruction. This dichotomy of increased or decreased permeability and porosity has clearly been documented in productive oil fields throughout the world and most notably in the

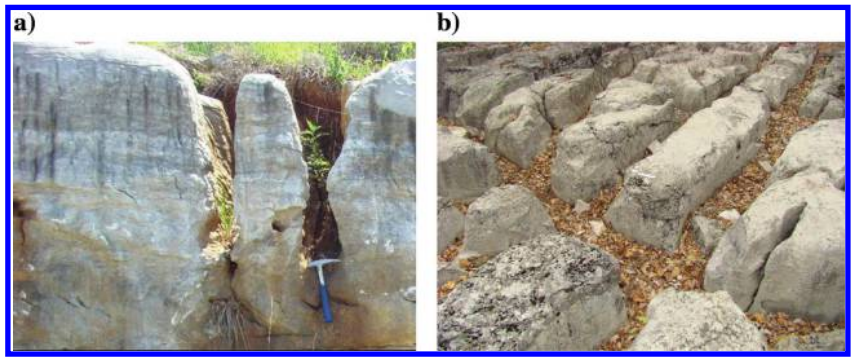

Figure 7. Grikes and clints showing vertical or near-vertical joint or fracture sets that have been solution enlarged. (a) The Ste. Genevieve Limestone; the hammer head is 18 cm (7 inch) long and (b) the Girkin Limestone; scale in photo is 15 cm (6 in). Both of these units were surveyed at the GRP. Photos from nearby Warren County, Kentucky.

U.S.A. in stratigraphic units such as the Ellenburger (Kerans, 1988), the San Andres (Tinker et al., 1995; Craig, 1988), and the Knox (Anderson, 1991). Many of the karst features documented in this study, such as the depressed bedrock surface oriented parallel to the Green River with several meters of relatively conductive sediment overlying bedrock, are probably attributable to solution enlarged vertical joints, similar to what Tinker et al. (1995) suggest for the San Andres reservoir in West Texas.

Suggested further studies

Studies conducted at the GRP are a work in progress. Undergraduate and graduate students from Western Kentucky University and Northern Kentucky University come to the preserve to learn geophysical methods and combine those with geologic properties and methods to develop big picture ideas for use in their future careers. The preserve provides an unprecedented workplace to implement a long-term program for developing a model for karst based petroleum exploration.

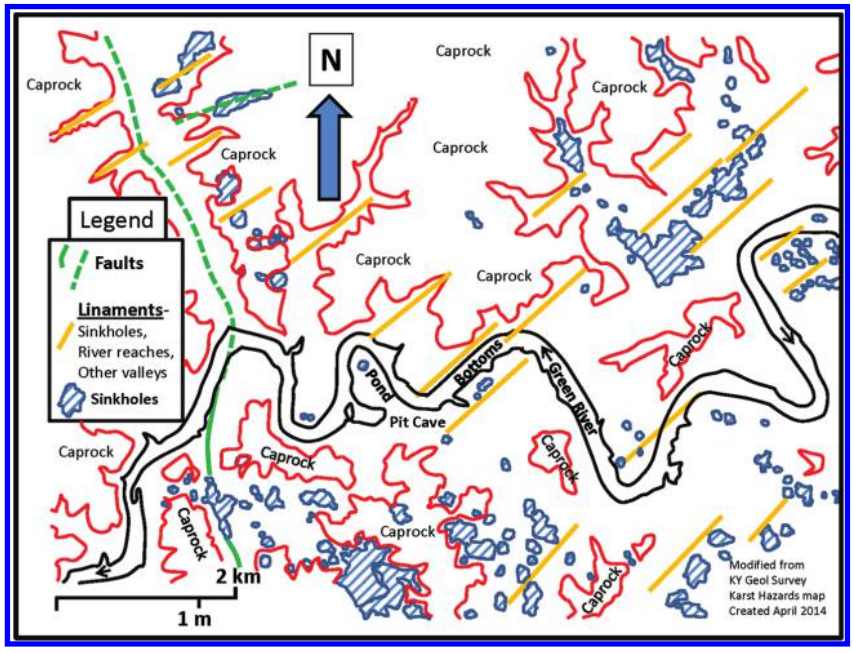

Figure 8. GRP region shown in context of a karst hazards potential map generated and modified from the Kentucky Geological Survey interactive map service (accessed April 2014). Blue diagonal marked areas are large sinkholes based on those exceeding contour interval (varies from 3 to 6 m [10–20 ft]) and areas at lower elevation below red lines demarcate high-karst geohazard potential corresponding to Ste. Genevieve and Girkin limestone exposures; areas at higher elevation designated Caprock have insignificant karst geohazards with exception of Haney Limestone exposure (not shown) but where eroded, provides karst windows and localized sinkhole hazards. Note alignment of sinkholes and karst valleys (lineaments) in northeast–southwest direction or parallel to a straight reach of the Green River in bottoms area surveyed: direction corresponding to regional joint patterns and these linear features contrast with less pronounced conjugates oriented 90° to northeast–southwest. Areas designated pond, pit cave, and bottoms correspond to three geophysical test beds described in the text (1–3 in Figure 3).

Future plans include the continued use of ERT and ReMi. Although 3D lines are instructive and assist in development of 3D "thinking," the 3D lines have a tradeoff between resolution and area covered. However, 2D lines can be combined into 3D images if the distance between the surveys is within 10%–15% of the electrode spacing (M. Lagmanson, personal communication, 2013). Additionally, recent developments in ERT technology (induced potential) using currents in the 6–30 A range can allow investigation of the subsurface in the 300-m (984-ft) range and more (M. Lagmanson, personal communication, 2013), allowing correlation of data obtained via use of near-surface geophysical methods to data derived through deeper methods. The use of closely spaced electrodes in the 2D and 3D ERT surveys will provide a more detailed image of the subsurface allowing better resolution of solution features, voids, and caves.

Drilling will always remain the method of choice for obtaining a correlation between the geologic and geophysical properties. Future plans are to obtain the Kentucky Geological Survey's Giddings rig and retrieve core samples along current and proposed ERT and ReMi lines to provide such data. The Laboratory for Applied Geophysics at Northern Kentucky University has a resistivity test box that allows testing of core samples. The measurements can easily be converted to ohm-m and entered into the model as a priori information. After modeling, the determination of the type and condition of the sedimentary infill of subsurface voids could be better ascertained, providing a better view of a potential oil reservoir.

In ERT studies conducted singularly, a competent limestone can have the same electric properties of a dry cave. ReMi studies are able to detect reversals at depth and can provide a cheap yet effective method to determine if the ERT signature represents a void or limestone.

The induced potential method (e.g., Butler, 2005, p. 265) has potential to assist in determining the composition of subsurface voids near chargeable materials. As a current is applied to a system (e.g., clay), it acts as a capacitor and the rate at which the current "drains" away is dependent on the material (in this case, water or air) it drains into (Butler, 2005). Water is a polar molecule and provides a pathway for the electrons to drain away, while air is resistive and provides no pathway.

Three-dimensional geocellular modeling or the concept of using models

to replicate and understand the reservoir in question (Deutsch, 2002; Shepherd, 2009) would work nicely in the karst regions of the GRP. The data collected at the GRP are not of sufficient quantity at this time to generate a geocellular model in the true sense of a reservoir because we only have collected seismic and resistivity data with no direct lithologic data or facies analysis in surveyed areas. As Pyrcz and Deutsch (2014, p. 10) note there necessarily needs to be an input of myriad data such as stratigraphic interpretations, outcrop data, petrophysical parameters such as porosity and K, and engineering data. However, long-term plans include determining regional trends of joints that may enlarge into pathways and reservoirs. We have begun to see the relationship with ERT and ReMi continuities or anomalies and how they relate to localized structural features such as joints and fractures (Figure 7) and lineaments that play into surface topography development such as alignment of dolines, formation of incised valleys, and parallelism with mapped fault zones (e.g., Figure 8). The area of investigation does tend toward 3D modeling. As the "picture" begins to develop following additional investigations, the modeling of the potential reservoir will be constructed not only to develop a sense of reservoir surfaces, conduits and geophysical data but also to assemble a 3D picture of the karst system. Karst systems and oil reservoirs require similar visualization techniques to be properly characterized. Geocellular modeling will bridge the divide between oil production and mitigation of karst hazards, demonstrating that conceptual models often cross disciplinary boundaries, creating a synergy of after effects.

Conclusions

This geophysical survey at the GRP using ReMi and ERT over proven and inferred modern karst features including pit caves, bedding plane-controlled caves or conduits, bedrock highs and lows at various scales, and associated karst infilling of sediments and fluvially derived sediments, provides a view of several measurable anomalies and continuities attributed to karst processes. Surveys along the Green River with ERT under drought and wetter than normal conditions resulted in mappable trends parallel to the modern river. Although the absolute values of ohm-m measurements along over half a dozen transects roughly perpendicular the river reflect varying soil moisture content, the ERT survey work coupled with the results of the ReMi surveys shows remarkably linear patterns that are parallel to the modern river. Additionally, these linear or rectilinear patterns can be noted regionally as doline or sinkhole defined linear features and karst valleys. Such linear features are consistent with regional joint and fractures systems and some fault systems and have been identified in many karst-linked oil prospects and Mississippi Valley type ore bodies in the Knox Group dolomites in south central Kentucky. Results of these geophysical field studies in a modern karst landscape in the Ste. Genevieve and Girkin carbonate units can form the basis for better understanding important paleokarst reservoirs throughout the world.

Acknowledgements

Thanks go to A. and O. Meier at Western Kentucky University for access to and encouragement of our research on the Green River Preserve. Special thanks go to the National Science Foundation for funding for equipment purchase to Brackman for the geophysical survey equipment used in this study. We also thank our Western Kentucky University and Northern Kentucky University students who over the years have worked diligently in the field during data acquisition. We also thank S. Pullammanappallil for assistance with the ReMi data processing.

References

Anderson, W. H., 1991, Mineralization and hydrocarbon emplacement in the Cambrian-Ordovician Mascot Dolomite of the Knox Group in south-central Kentucky: Kentucky Geological Survey, vol. 4, *of* Report of Investigations: 11.

Boore, D., 2003, Simulation of ground motion using the stochastic method: Pure and Applied Geophysics, **160**, 635–676, doi: 10.1007/PL00012553.

Borden, J. D., and R. W. Brucker, 2000, Beyond Mammoth Cave — A tale of obsession in the world's longest cave: Southern Illinois Press.

Brackman, T., S. Johnson, S. Rouse, and S. Pullammanappallil, 2011a, Using LiDAR and ReMi for location and delineation of landslides in northern Kentucky: Presented at the AEG Annual Meeting.

Brackman, T., S. Pullammanappallil, and J. Rockaway, 2011b, Using ReMi inside and out at a tunnel site in northern Kentucky: Presented at the AEG Annual Meeting.

Brucker, R. W., and R. A. Watson, 1976, The longest cave: Southern Illinois Press.

Butler, D. K., 2005, Near-surface geophysics: SEG Investigations in Geophysics 13.

Craig, D. H., 1988, Caves and other features of Permian karst in San Andres dolomite, Yates Field Reservoir, West Texas, *in* N. P. James, and P. W. Choquotte, eds., Paleokarst: Springer-Verlag, 342–363.

Deutsch, C. V., 2002, Geostatistical reservoir modeling: Oxford University Press.

Granger, D. E., D. Fabel, and A. N. Palmer, 2001, Pliocene — Pleistocene incision of the Green River, Kentucky determined from radioactive decay of cosmogenic ^{26}Al and ^{10}Be in Mammoth Cave sediments: Geological Society of America Bulletin, **113**, 825–836, doi: 10.1130/0016-7606(2001)113<0825:PPIOTG>2.0.CO;2.

International Code Council, 2000, The 2000 ICC International Building Code.

Jacoby, B. S., E. W. Peterson, T. Dogwiler, and J. C. Kostelnick, 2011, Estimating the timing of cave level devel-

opment with GIS: Speleogenesis & Evolution of Karst Aquifers, **11**, 52–61.

Joyner, W. B., R. E. Warrick, and T. E. Fumal, 1981, The effect of Quaternary alluvium on strong ground motion in the Coyote Lake, California, earthquake of 1979: Bulletin of the Seismological Society of America, **71**, 1333–1349.

Kerans, C., 1988, Karst-controlled reservoir heterogeneity in Ellenburger Group carbonates of West Texas: AAPG Bulletin, **72**, 1160–1183.

Koefoed, O., 1979, Geosounding principles: Resistivity sound measurements, Methods in Geochemistry and Geophysics 14: Elsevier Science Ltd.

Liu, H. P., D. M. Boore, W. B. Joyner, D. H. Oppenheimer, R. E. Warrick, W. Zhang, J. C. Hamilton, and L. T. Brown, 2000, Comparison of phase velocities from array measurements of Rayleigh waves associated with microtremor and results calculated from borehole shear wave velocity profiles: Bulletin of the Seismological Society of America, **90**, 666–678, doi: 10.1785/0119980186.

Loke, M. H., J. E. Chambers, D. F. Rucker, O. Kuras, and P. B. Wilkinson, 2013, Recent developments in the direct-current geoelectrical imaging method: Journal of Applied Geophysics, **95**, 135–156, doi: 10.1016/j.jappgeo.2013.02.017.

Loucks, R. G., 1999, Paleocave carbonate reservoirs: Origins, burial-depth modifications, spatial complexity, and reservoir implications: AAPG Bulletin, **83**, 1795–1834.

Loucks, R. G., 2001, Modern analogs for paleocave-sediment fills and their importance in identifying paleocave reservoirs: Gulf Coast Association of Geological Societies Transactions, **51**, 195–206.

Louie, J. N., 2001, Faster, better: Shear-wave velocity to 100 meters depth from refraction microtremor arrays: Bulletin of the Seismological Society of America, **91**, 347–364, doi: 10.1785/0120000098.

May, M. T., 2013, Oil-saturated Mississippian-Pennsylvanian sandstones of south-central Kentucky, *in* F. J. Hein, D. Leckie, S. Larter, and J. R. Suter, eds., Heavy-oil and oil-sand petroleum systems in Alberta and beyond: AAPG Studies in Geology 64, 373–405.

May, M. T., and K. W. Kuehn, 2009, Renewed interest in heavy oils and rock asphalt in south central Kentucky: World Oil, **230**, 65–59.

McMechan, G. A., and M. J. Yedlin, 1981, Analysis of dispersive waves by wave field transformation: Geophysics, **46**, 869–874, doi: 10.1190/1.1441225.

Meiman, J., C. Groves, and S. Herstein, 2001, In-cave dye tracing and drainage basin divides in the Mammoth Cave karst aquifer, Kentucky, *in* E. L. Kuniansky, ed., Geological survey karst interest group proceedings, water-resources investigations: USGS, 179–185.

Merino, E., and A. Banerjee, 2008, Terra rossa genesis, implications for karst, and eolian dust: A geodynamic thread: Journal of Geology, **116**, 62–75, doi: 10.1086/524675.

Nelson, W. J., 1990, Structural styles of the Illinois basin, *in* M. W. Leighton, D. R. Kolata, D. F. Oltz, and J. J. Eidel, eds., Interior cratonic basins: AAPG Memoir 51, 209–246.

Nissen, S. E., J. H. Doveton, and W. L. Watney, 2008, Petrophysical and geophysical characterization of karst in a Permian San Andres reservoir, Waddell Field, West Texas: Kansas Geological Survey, Open-file report, 2008-5.

Noger, M. C., 1987, Tar-sand exploration in Kentucky, *in* R. F. Meyer, ed., Exploration for heavy crude oil and natural bitumen: AAPG Studies in Geology 25, 521–536.

Palmer, A. N., 1981, A geological guide to Mammoth Cave National Park: Zephrus Press.

Palmer, A. N., 1987, Cave levels and their interpretation: The National Speological Society Bulletin, **49**, 50–66.

Palmer, A. N., 1991, Origin and morphology of limestone caves: Geological Society of America Bulletin, **103**, 1–21, doi: 10.1130/0016-7606(1991)103<0001:OAMOLC>2.3.CO;2.

Palmer, A. N., 1998, Unpublished stratigraphic column of Mammoth Cave area.

Pyrcz, M. J., and C. V. Deutsch, 2014, Geostatistical reservoir modeling: Oxford University Press.

Quinlan, J. F., and R. O. Ewers, 1981, Hydrogeology of the Mammoth Cave region, Kentucky: Field trip guidebook: Geological Society of America, 8, 457–506.

Quinlan, J. F., and J. A. Ray, 1981, Groundwater basins in the Mammoth cave region, Kentucky, showing springs, major caves, flow routes, and potentiometric surface: U.S. National Park Service, Mammoth Cave, KY — Friends of Karst, Occasional Paper, 1 (Map).

Quinlan, J. F., and J. A. Ray, 1989, Groundwater basins in the Mammoth Cave region: U.S. National Park Service, Mammoth Cave, KY — Friends of Karst, Occasional Paper, 2 (Map).

Ray, J. A., and J. C. Currens, 1998, Mapped karst groundwater basins in the Campbellsville 30 × 60 minute quadrangle: Kentucky Geological Survey, Map and Chart Series 17, Series XI, 1:100,000 scale.

Revil, A., M. Karaoulis, T. Johnson, and A. Kemna, 2012, Some low frequency electrical methods for subsurface characterization and monitoring in hydrogeology: Hydrogeology Journal, **20**, 617–658, doi: 10.1007/s10040-011-0819-x.

Rucker, M., 2007, Integrating seismic refraction and surface wave data collection and interpretation for geotechnical site characterization: Presented at the FHWA Highway Geophysics Conference.

Schwartz, B. F., M. E. Schreiber, and T. Yan, 2008, Quantifying field-scale soil moisture using electrical resistivity imaging: Journal of Hydrology, **362**, 234–246, doi: 10.1016/j.jhydrol.2008.08.027.

Shepherd, M., 2009, 3-D geocellular modeling, *in* M. Shepherd, ed., Oil field production geology: AAPG Memoir 91, 175–188.

Slater, L., 2007, Near surface electrical characterization of hydraulic conductivity: From petrophysical properties to aquifer geometries — A review: Surveys in Geophysics, **28**, 169–197, doi: 10.1007/s10712-007-9022-y.

Sweeting, M. M., 1973, Karst landforms: Columbia University Press.

Thorson, J. R., and J. F. Claerbout, 1985, Velocity-stack and slant-stack stochastic inversion: Geophysics, **50**, 2727–2741, doi: 10.1190/1.1441893.

Tinker, S. W., J. R. Ehrets, and M. D. Brondos, 1995, Multiple karst events related to stratigraphic cyclicity: San Andres Formation, Yates field, West Texas, *in* D. A. Budd, A. H. Saller, and P. M. Harris, eds., Unconformities and porosity in carbonate strata: AAPG Memoir 63, 213–238.

Toomey, R. S., and R. Olson, 2008, USGS field guide, http://pubs.usgs.gov/sir/2008/5023/pdf/44toomey.pdf, accessed 13 March 2014.

White, W. B., 2007, Cave sediments and paleoclimate: Journal of Cave and Karst Studies, **69**, 76–93.

Michael T. May received B.S. and Ph.D. degrees from Indiana University and an M.S. from the University of Kansas. He is a professor of geology and the geology program leader at Western Kentucky University, where he has been teaching various sedimentologic, stratigraphy, and petroleum geology related courses, as well as environmental geology and aqueous geochemistry since 1996. He is also a consultant in the energy and environmental sectors. Prior to his academic appointment he worked for two environmental consulting companies in Kansas and for Exxon and Shell Oil in Texas. His recent research interests include geophysical and stratigraphic characterization of modern and paleokarst landscapes, stratigraphic hiatus problems, and the role of diagenesis in reservoir compartmentalization. He is a registered professional geologist in the Commonwealth of Kentucky and a registered geologist in Indiana.

Thomas B. Brackman received a B.S. in the geological sciences from the University of Kentucky and an M.S. in earth science from the University of Memphis. He is a registered professional geologist in the Commonwealth of Kentucky. He has worked as a research scientist, a hydrogeologist at an environmental consulting firm, and as a research hydrogeologist at Western Kentucky University. He currently serves as the Laboratory for Applied Geophysics director at Northern Kentucky University for the Center for Integrative Natural Science and Mathematics. This involves recruiting students to science, technology, engineering, and mathematics degrees, lecturing for geophysics classes in the Department of Physics and Geology, and conducting applied geophysical research. His current research interests include the use of ReMi techniques and electrical resistivity tomography as they apply to delineating landslides and understanding subsurface features of karst.